Unmanned Aerial System for deployment and recovery of research equipment at sea

Artur Zolich, Tor Arne Johansen
Norwegian University of Science and Technology,
Center for Autonomous Marine Operations and Systems,
Department of Engineering Cybernetics, Trondheim, Norway,
{artur.zolich,tor.arne.johansen}@ntnu.no

Moustafa Elkolali, Ahmed Al-Tawil, Alex Alcocer
Oslo Metropolitan University,
Department of Mechanical, Electronic
and Chemical Engineering, Oslo, Norway,
{elkolali,ahmedalt,alepen}@oslomet.no

Abstract—In this paper we present details of Miniature Underwater Gliders (MUG) deployment and recovery mechanism using a multirotor Unmanned Aerial Vehicle (UAV). The paper discusses details of MUG localization with computer vision, pick-up algorithm, and recovery mechanism.

I. Introduction

Recent developments in sensor technology and unmanned vehicles pave the way for new methods for observation of water environment and its research [1], [2]. Unmanned Aerial Vehicles (UAVs) are utilized for activities such as aerial imaging [3], or water sampling [4]. Unmanned Surface Vehicles (USV) are used to monitor water environment [5]. Underwater robots can collect data from the water column, seabed or survey infrastructure [6], [7]. Several types of vehicles can be combined into a multi-robot system-of-systems, where the constituent systems provide unique features and enables new scenarios for collection of environmental data at given geographical location [8], [2]. Examples are operations which benefits from physical interaction between Unmanned Systems. USVs have shown their potential in delivery of slower underwater units to a designated area [9]. Similarly, recovery and deployment of objects using UAVs can reduce vessel use of time, or allow to run the entire operation from the shore.

Utilization of multiple vehicles creates another opportunity. For example a group of low-cost Miniature Underwater Gliders (MUGs) can scan the water column in multiple locations simultaneously, preparing maps of environmental parameters. However, underwater gliders have some limitations that need to be addressed. They are propelled by a variable buoyancy system, and a force generated by wings during dive and ascend. Their vertical speed is low and they require sufficient depth for operation. Deployment from shore can be challenging, and vehicles are usually deployed directly in the area of interest by a crew on a boat or vessel.

In this paper we propose a MUG recovery and deployment mechanism, where a multirotor UAV serves as a MUG carrier, [10]. Multirotor UAVs, as Vertical-Take-Off-and-Landing (VTOL) platforms, are capable of precise maneuvers and hover. The UAV can deploy and recover MUGs in situations where otherwise it would be challenging. Examples are operations nearby a moving ship where MUGs can hit the hull, or directly from shore where water is too shallow. UAV endurance allows to distribute and collect MUGs in a radius of a few kilometers – a distance which the MUG would otherwise traverse in a few days.
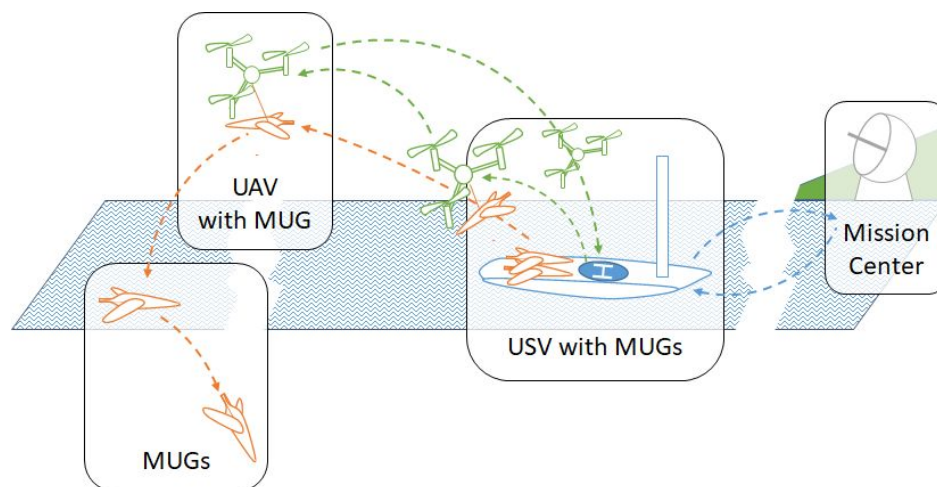

Fig. 1: System concept

Key contributions of this paper are: (1) an overview of novel system-of-systems for marine research; (2) an UAV machine vision system with an efficient color filtration method showing improved computational performance for MUG detection; (3) the design of a mechanism for recovery of objects from the sea surface.

Section II of this paper describes system components while Section III provides details on MUG localization and pick-up algorithms.

II. System overview

The system is designed to perform a fully-autonomous operation, where MUGs are deployed from a long endurance USV (Fig. 1). Since the USV and MUGs have limited maneuverability and speed, an UAV is used to deploy and recover MUGs.

In our use case we assume following requirements: (1) The MUG will be deployed and recovered within 1 km from the hosting USV. That allows to reduce the UAV charging time between flights and reduce the UAV weight – thanks to a smaller battery. (2) The area is clear from obstacles, e.g. wind farms. The UAV can fly to the MUG in a straight line without an obstacle avoidance system on-board. (3) The water is clear from other equipment, e.g. fishing nets and buoys that could entangle the MUG. (4) The recovery operation should be performed in a good weather conditions and calm sea, preventing an adverse wave hit during the UAV touchdown on water.

The proposed system consists of three core, interrelated elements. A Robotic Base Station (RBS) – allowing to handle MUGs on-board the USV, the UAV, and MUGs.

A. Miniature Underwater Glider

The current MUG prototype has a total length of 1.5m, a wingspan of 0.4m, a total weight of 7kg and maximum operating depth of 750m. The hull of the glider was designed from carbon fiber reinforced polymers (CFRP) and manufactured using filament winding in order to be able to withstand the external pressure. CFRP material was chosen for the design over traditional metals, such as Aluminum, due to its high strength to weight ratio. Hence satisfying the depth requirement without exceeding the weight constraint set by the UAV lifting capabilities. The glider utilizes a small hydraulic system, as a variable buoyancy system (VBS). The system consists of a micro hydraulic pump actuated by a brushless DC motor, an internal tank with a feedback system, and an external bladder to change the total buoyancy of the vehicle. The system was tested at different pressures using a hyperbaric pressure vessel and a tailor-made test rig. There are other mechanical components of the vehicle that are required for the navigation and control of the vehicle, such as a power screw mechanism to trim the pitch angle of the glider, and another mechanism for the roll angle adjustment. The glider performs a 180° rolling rotation at each buoyancy state because it has a tapered non-symmetric wing profile, which was proven to be more efficient [11]. The onboard batteries, which serve also as the moving mass for the pitch and roll mechanisms, are 6S2P Lithium Ion that weighs 0.4kg and has a power capacity of 6.5Ah. A Battery Management System (BMS) circuit was to convert the supply voltage to different voltage outputs depending on the need of different components, circuits, and sensors, as well as handle battery charging and protection. A total of 13 electronic circuits are used in the glider, with different applications for each of them, such as power management, telemetry management, communication, motors control, VBS control, navigation, scientific payload operation, data storage, safety measures, etc. All circuits were custom designed and manufactured to be optimized in weight and power consumption. The vehicle has different communication interfaces depending on its location and the user proximity. Wi-Fi and LoRa are used in the case of short-range communication and data retrieval, while 4G and satellite are used in the case of long-range communication. The scientific payload includes temperature and pressure sensors as well as a fluorometer manufactured by TriOS gmbh to measure chlorophyll concentration. There are other onboard sensors, used to provide feedback from different system components, such as shaft encoders and linear potentiometers, and feedback about different parameters of the glider state and orientation such as an Inertial Measurement Unit (IMU) and an altimeter. The vehicle is divided into two separate subsections. The back section contains the scientific payload, batteries, mechanisms, wings, and antennas, while the front one contains the variable buoyancy system. The two sections are connected by a middle cap. This design

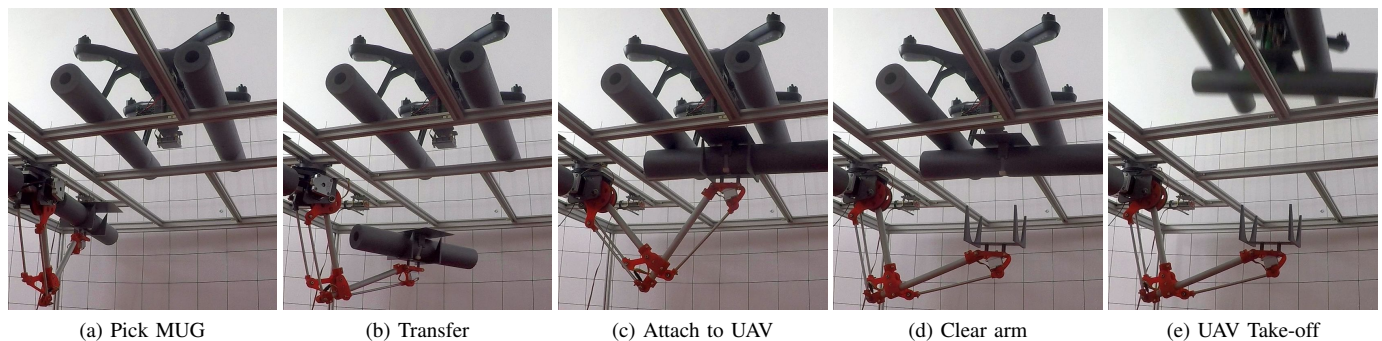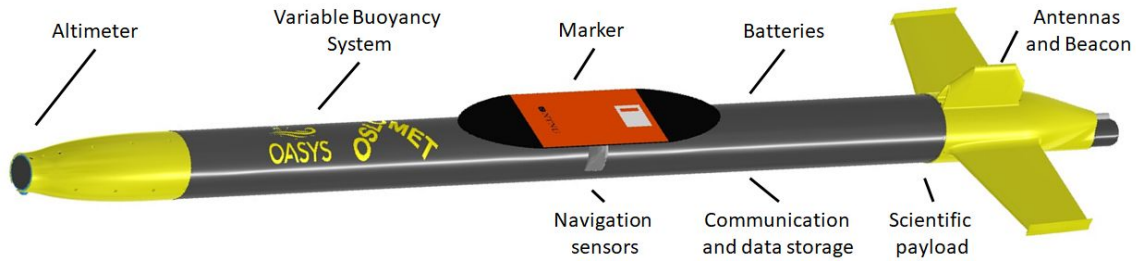| (a) Pick MUG | (b) Transfer | (c) Attach to UAV | (d) Clear arm | (e) UAV Take-off |

Fig. 2: Robotic arm action

Fig. 3: Elements of the MUG

was adopted to allow the user to open the glider from the middle to ensure easy maintenance and data collection. A CAD model of the glider is shown in Fig. 3.

B. Robotic Base Station

The RBS is based on a light-weight and modular frame of standardised aluminum construction elements, which allows easy transportation and integration on a floating platform. The RBS provides a landing pad to the UAV, manipulates MUGs, and provides additional services, such as access to wireless power source. It also accommodates a computer running control algorithms for the UAV and motion sequence of a robotic arm. The centerpiece of RBS is a robotic arm. Currently the arm is a 3 Degrees of Freedom (DoF), palletizer-type robot based on an open-hardware uStepper Robot Arm Rev 4 design (uStepper, Denmark). The arm is controlled with an Arduino embedded computer which handles arm kinematics, and drives stepper motors through a dedicated CNC Shield. A certain limitation of the robotic arm is limited payload weight it can handle. For heavier items, e.g. a full size MUG, arm could be replaced with, e.g. a custom XYZ Cartesian robot.

Two independent slots are provided for MUG storage. Thanks to the modular design, the number of slots can easily be increased. Each slot is equipped with an Electro-Permanent Magnet that keeps MUG in position. The work envelope of the robotic arm allows to implement additional features in the design. For example, the arm can deliver wireless charging transmitter to a given position in order to charge MUGs or the UAV. Highlights of the robotic arm

delivering a MUG-dummy from one of the storage slots to the UAV is presented on Fig. 2.

C. Unmanned Aerial Vehicle

The full-scale system uses the UAV octocopter based on SpreadingWings S1000 (DJI, China) frame and propulsion systems, with added avionics based on Pixhawk autopilot and ArduCopter firmware (Fig. 4b). The high-level control of the UAV is realized through the LSTS toolchain [12].

During the step-wise design process we have used a range of UAVs and tools that helped us to address and solve challenges specific to certain phases of the system development. Tools such as ArduCopter autopilot Software-In-The-Loop (SITL) simulator can be a relevant replacement for data collected with a physical vehicle, Especially if combined with additional tools, e.g. FlightGear that can simulate the camera view from the UAV, and manipulate objects in the scenery. These features allow to test new algorithms and functions in safe, simulated environment before proceeding to field-trials. However, artificial images generated in the simulator may not mimic output of optical instruments (cameras) of the UAV realistically. Physical camera images contains phenomenon which are not always present on the output of graphics engines of open-source SITL platforms. These can be, e.g. noise, glare, water splashes, shadows, reflections, data-transfer delays and bitrate fluctuations. One solution to that is use a video footage recorded during the UAV flight for tuning of the image processing algorithm. Next step can be hardware-in-the-loop tests on a low-cost indoor platform (Fig. 4a).

(a) Prototyping on Ryze Tello

(b) Line-capture trial with DJI S1000

(c) Release by EPM mechanism on 3DR Solo

Fig. 4: UAVs used during system development and testing

In our work we used all of these above mentioned methods before proceeding to tests with an outdoor UAV. Outdoor testing was mainly conducted using a compact Solo (3D Robotics, USA) quadrocopter with a modified software - OpenSolo4 (Fig. 4c). The hardware of Solo autopilot is similar to the one used on S1000 UAV, and they both run the same version of ArduCopter firmware which is crucial for consistent results. Due to its size Solo is easier to handle during field trials, and therefore is used more frequently to test the system. Firmware version may have an impact on reaction to inputs and the UAV behaviour. Comparison of both platforms during the field trials shows that thanks to the common autopilot software Solo and S1000 UAVs reactions to control algorithms are similar.

D. Deployment and recovery mechanism

The MUG deployment and recovery mechanism has been design and tested through an iterative process (Fig. 4). The initial concept assumed that the MUG will be captured by the UAV with a line. The hook - located on a MUG's vertical fin - got attached to a line spread between the UAV landing skids. Field trials showed, that this approach requires very high precision in the UAV control and put risk on both MUG and UAV. If the line misses the hook, it may wrap around other parts of MUG. Moreover, the hook forced a certain UAV approach direction and path, which makes it challenging when MUG moves on water surface.

A new concept evolved utilizing Electro-Permanent Magnet (EPM). EPM is a device in which an external magnetic field can be switched on and off using electric current. In our design we use EPM V3 R5C (NicaDrone, Nicaragua), based on an open-hardware OpenGrab design. A key benefit of EPM over electromagnet is that only a short power burst is required only to change the magnet state. In order to keep the EPM's magnetic field in a steady state only a limited power is required (ca. 50mW). Turn on-off cycle time is 0.75-1.2s, with peak current of ca. 1A at 5V power supply. Typical maximum holding force is declared to be 300N. The available EPM requires waterproofing, after which it allows capturing and releasing submerged metal objects.

The UAV is equipped with the EPM while MUG wing contains a 200x100 mm metallic surface (Fig. 3). A certain benefit of the new method is that UAV can approach the MUG from any direction which reduce risks for both the UAV and the MUG. Moreover, several EPMs can be chained together into an array. That increases active capture area, which relaxes requirements on the UAV approach accuracy.

III. MINIATURE UNDERWATER GLIDER LOCALIZATION AND IDENTIFICATION

The UAV is able to localize and approach the MUG on the surface of the water thanks to GNSS data and a vision system. When the MUG surfaces, it is expected to send its geographic position from GNSS over 4G or Iridium network to the server, from which the data can be retrieved by the UAV via an Internet connection. Then the UAV can fly to the location reported by the MUG for its recovery.
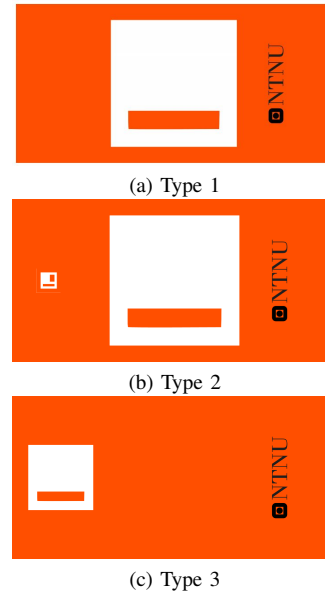

(a) Type 1

(b) Type 2

(c) Type 3

Fig. 5: Marker iterative designs

The reported MUG's GNSS position does not provide sufficient accuracy to retrieve the vehicle. First, MUG is equipped with regular COTS receiver without additional features such as RTK. Second, the GNSS antenna is very close to the sea surface, which may compromise the precision and availability of measurements. Moreover, the MUG position may keep changing, e.g. due to sea current or wind.

Therefore, for precise guidance towards the surfacing MUG the UAV utilizes a machine vision system. The MUG is equipped with a marker, which is described in the following section. The UAV is equipped with a regular daylight, COTS, RGB camera with a wide angle lens. In most of the experiments we found it sufficient to use a 720p (1280x720 px) camera with a lens of focal length equivalent of 21.9 mm - horizontal field of view (FOV) of 94.4 deg, and vertical FOV of 55 deg. The system is flexible, and camera parameters can be changed. When the UAV reaches the provided GNSS location, a dedicated algorithm controls the UAV descent towards the marker. The descent is a multi-stage process, where each stage is using different optical feature of the marker.

A. Marker design

The marker on the MUG has 2 navigation aids - for coarse and precise navigation. For the coarse navigation the majority of the marker area is painted in "International Orange" (FF4F00) color. The color is used in industry to increase objects visibility on the water surface. For the fine navigation within a short distance between vehicles, an Aruco tag – with id 0 – is printed on top of the marker. Aruco tag code recognition is also used to confirm that the object towards which the drone descends is a MUG. There may be other object with similar color (e.g. fishing net buoy) in the area which the UAV should not attempt to recover.

In our design the Aruco tag has been intentionally modified to better fit our use case (Fig. 5). The regular tag with id 0 is mostly black rectangle with a white bar inside. Under certain conditions camera can register bright sun reflections from marker surface – captured as white spots on the image. That may impact Aruco code recognition. In our approach we use a negative of the Aruco tag pattern. Thanks to that the major part of the tag is white, so the bright sun reflections in that area should not affect pattern recognition significantly. Next modification is change of the black Aruco tag elements with "International Orange". That increases the area of that color on the marker, therefore making it easier to be detected from higher altitude.

Three marker patterns were tested (Fig. 5). Initially an 80 mm Aruco tag was printed in the center of the marker. During steady UAV maneuvers that size allowed to recognize the Aruco tag from an altitude of ca. 5 meters. However, at the last stage of descend the marker was filling almost entire camera image, and its edges often left the camera view. To solve that, in a second iteration (Fig. 5b), additional 10 mm tag was placed on a side of the marker. That additional feature was often blurred due to the UAV vibrations, and did not provide satisfactory results. A compromise, and final design is presented on (Fig. 5c). The control algorithm can recognize a new, 40 mm tag from a satisfactory altitude of ca. 3 meters, and it is able to track it to the touchdown. A positive side effect of that design is further increase of the "Intenrational Orange" area on the marker, so it is better visible from a higher altitude.

B. Color detection

A color detection algorithm is needed for coarse localization of the marker. Two types of color filter were examined. First, the marker color detection based on a typical HSV color filter was tested. To tune the filter we used 84 pictures of the marker taken throughout a day. Parts of the images with marker details were analysed to get expected H, S, and V ranges (Fig 6). The result was a color filter set between HSV(1, 78, 32) and HSV(30, 205, 255).

However, another approach prove better computational performance with similar result. Our UAV camera captures data represented in an RGB color space. In our scenario we focus on the water surface environment and high-contrast objects. Our hypothesis was that color filtering using RGB channels data directly, will be more computationally efficient than filters requiring conversion to HSV color space. A satisfactory result for "International Orange" color detection on image was achieved with a weighted combination of RGB channels data:

$$Monochrome = Red - 0.7 \cdot Green - 0.3 \cdot Blue. \quad (1)$$

and further processing the output with 5x increase of brightness, followed by pixel value threshold to zero for values lower than 250.

The comparison of outputs of both HSV and RGB filter effects applied on a full color palette is shown on Fig. 7. To evaluate the performance of both methods we used watercarft aerial images from MASTI-v2 dataset [13] -
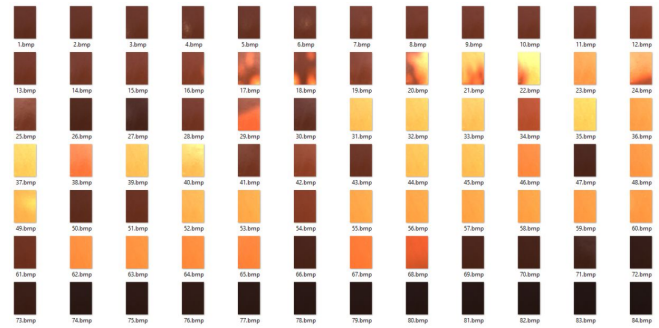
(a) Marker detail throughout the day
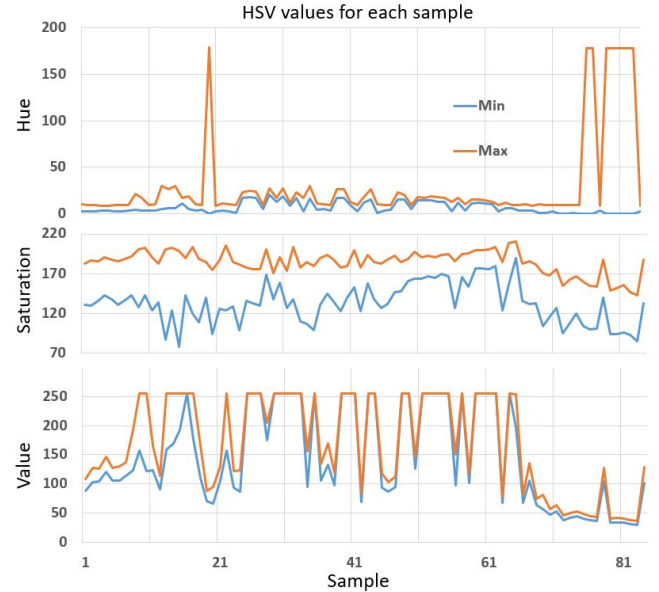
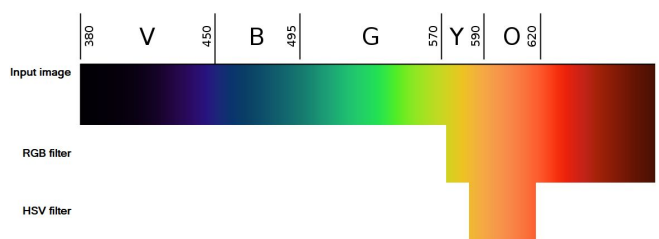(b) HSV graph

Fig. 6: Marker color throughout the day

Fig. 7: Color filters output

"detail' subset containing 1789 images with size of 512x512 px. Comparison of both methods has been performed using a custom test software (C#, Emgu.CV 4.3.0.3890). Test run on Dell Latitude 5414, Intel(R) Core(TM) i7-6600U CPU 2.81 GHz, 16 GB RAM running Windows 10.

A 100 iterations of the each HSV and RGB based methods were performed in changing order. For performance comparison a time of execution of the key parts of the code were recorded. For RGB filter, following code execution time was measured:
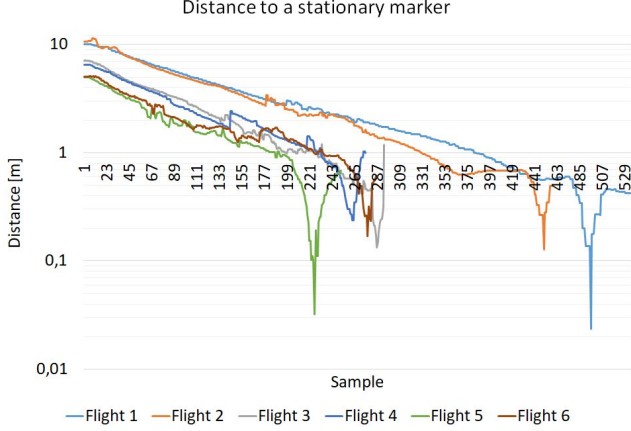
Distance to a stationary marker

Fig. 8: UAV approach accuracy to a stationary marker
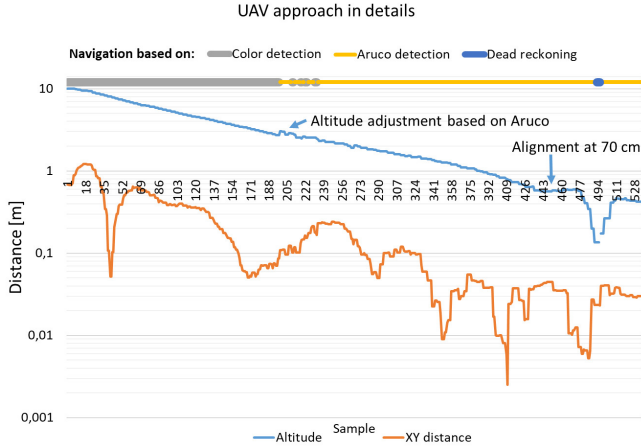
UAV approach in details

Fig. 9: UAV approach - detailed

```
fChannels = fSource.Split();
frGray = fChannels[2]
        − 0.7 ∗ fChannels[1]
        − 0.3 ∗ fChannels[0];
CvInvoke.Threshold(frGray, frDst,
    50, 255,
    Emgu.CV.CvEnum.ThresholdType.ToZero);
```

while for HSV filter:

```
CvInvoke.CvtColor(fSource, frameHsv,
    ColorConversion.Bgr2Hsv);
CvInvoke.InRange(frameHsv,
    new ScalarArray(
        new MCvScalar(1, 78, 32)),
    new ScalarArray(
        new MCvScalar(30, 205, 255)),
    frameHsvMask);
```

Table I present the end results. The simplified method using RGB-data shows ca. 7% better performance. The performance may vary depending on various elements, such

TABLE I: Results of 100 iterations on dataset of 1789 images

	HSV	RGB
Average time [ms]	3118.87	2902.41
Std. dev. [ms]	140.58	145.78
Minimum time [ms]	3000.53	2685.32
Maximum time [ms]	4176.84	3380.23

as hardware platform, compiler settings, or OpenCV library version.

C. Aruco marker detection

The Aruco marker can be detected on an image with an *OpenCV* method (*cv::aruco::detectMarkers*). The processing, and therefore final result, can be controlled using *DetectorParameters* and input image pre-processing. As mentioned in Section III-A the visual features of the Aruco tag on the MUG marker were modified. Therefore, each drone's camera frame is converted to a negative to restore a correct Aruco color scheme. The default *DetectorParameters* give satisfactory results for most of the processed frames. To prevent from false-negatives, for frames on which Aruco tag is not detected a second check is performed. In some cases when the first method fails, the Aruco marker can be detected if the source frame is modified by applying *MEAN C* type *Adaptive Binary Inverted Threshold* with *max value* of 255, *block size* of 599, and and *C* of 0.

D. MUG pick-up procedure

The MUG pick-up procedure is shown on Fig. 10. In our setup the image processing algorithm is able to recognise the color marker from an altitude between 15 and 20 meters. The algorithm separates the "International Orange" object in the image, assuming it is a marker, and computes its geometric parameters such as center of contour (centroid). Then the UAV descends with a fixed velocity, adjusting the X and Y axes position to keep the centroid in the middle of the camera image. At the altitude of 1.5 meters, the algorithm expects to identify the Aruco tag. If it fails, the procedure is aborted. If it is successful, the Aruco tag provides precise information of XYZ distance between the UAV and MUG, as well as Euler angles between the vehicles.

Although two methods are used to detect Aruco tag in the camera image, an additional dead reckoning mechanism is added. If an Aruco marker has been detected on previous frames but is not in the following images a dead reckoning algorithm allows to continue maneuver for a limited amount of time. The mechanism integrates XYZ velocities reported by the UAV over time to calculate position shift from last decoded XYZ positions of Aruco tag. The output is valid by a limited time, e.g. 3 seconds. Within that time a new Aruco detection needs to be successful, otherwise the drone climbs and repeat the procedure.

During descent the accurate Z distance readout of Aruco tag detection method overrides the barometric altitude reading of the UAV's sensors, and is used further as the UAV altitude reference. Next, the UAV aligns its heading with
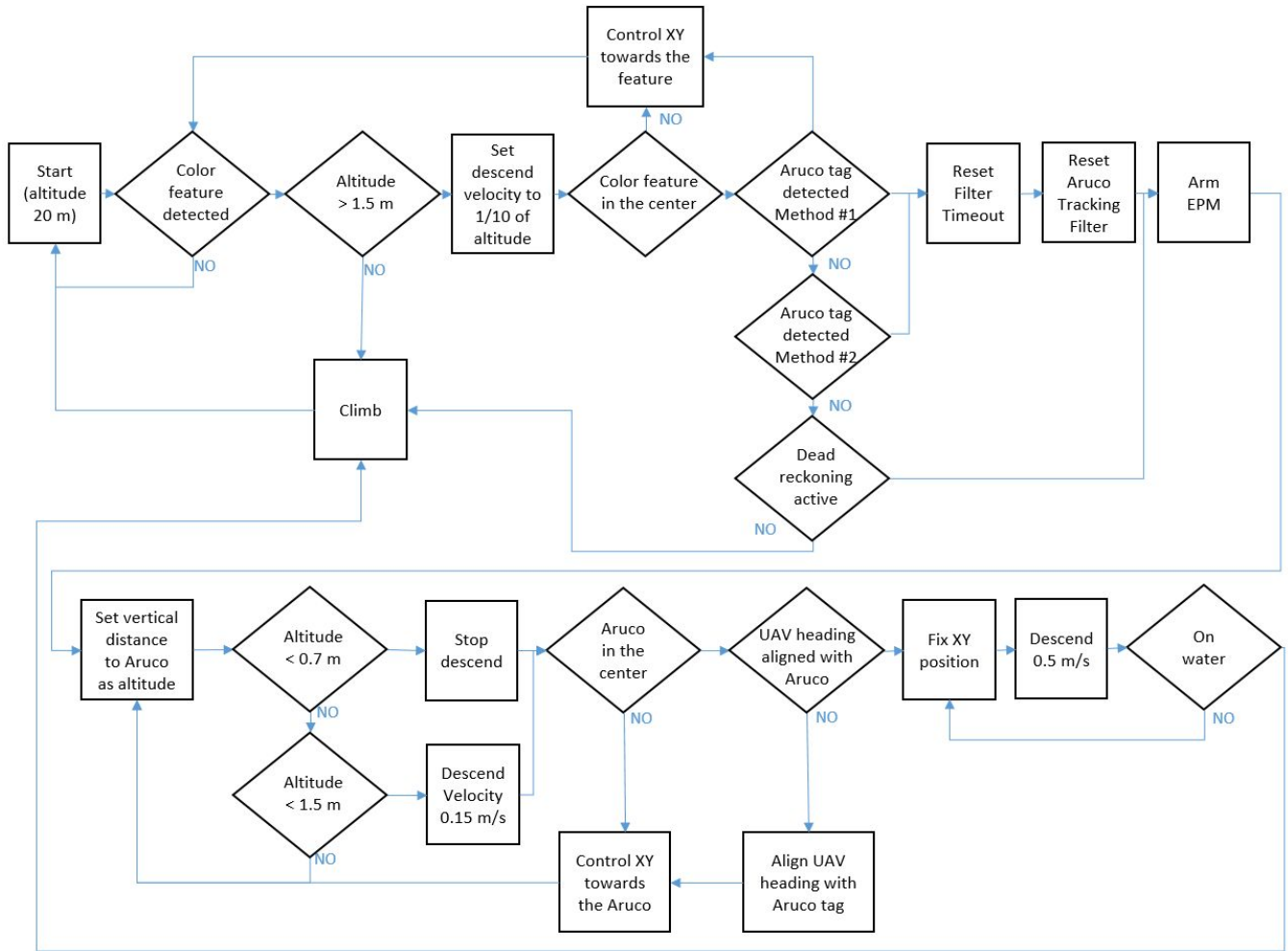
Fig. 10: Pick-up algorithm

the marker, while continuing descend. The descend rate is computed as 1/10th of current altitude, but not lower than 15 cm/s. At an altitude of 70 cm above the marker, the UAV reaches the last stage of descend. The closer the UAV is to the ground, the more propulsion downwash is reflected from the ground surface. That can impact precision of control and cause the UAV to drift aside. The MUG can drift as well when exposed to the additional airflow. Therefore it is crucial that the touchdown is executed quickly and with limited position corrections. At this stage the UAV aligns with the Aruco tag, trying to reduce the XY velocities to below 5 cm/s. Empirical tests show that lower velocity at this stage, e.g. 1 cm/s, produces better landing accuracy, but the condition is often too hard to reach within satisfactory flight time. When the velocity condition is met, the XY control is zeroed and the UAV executes a dynamic descend at 50 cm/s until it reaches the sea surface - condition indicated by a separate sensor. The successful pick-up is confirmed by a separate sensor, an end-switch.

Fig. 8 presents the approach precision with a stationary marker, performed by the Solo UAV (Fig. 4c). Each data-line shows distance to the marker calculated by the vision algorithm during an individual descend. The minimum values represent distance to the Aruco marker at touchdown. In presented examples the UAV touched down 3 mm to 17 cm off the marker center. Fig. 9 shows a single approach in more details. In the showcased run, the UAV detects the marker and starts to descent at an altitude of ca. 10 m. The initial horizontal shift from the marker, calculated based on the color recognition, is ca. 67 cm. The UAV descent and maneuver to align the marker with the center of the camera image. At ca. 3 meters the Aruco marker is detected, and Z distance overrides the UAV barometric altitude readout. Descend continues based on Aruco marker to an altitude of 70 cm. When requirements for Aruco position towards camera center is satisfied the final phase of 50 cm/s descend activates. As a note a dead reckoning on the graph activates for a moment when Aruco marker fail to be detected in the image. However, in that flight-phase its output is neglected as shown on Fig. 10.

IV. FUTURE WORK

The presented work shows status of ongoing activities on Unmanned Aerial System for deployment and recovery of

research equipment at sea. Currently key system components are developed individually. Next phase will be integration and further demonstrations of key scenarios in relevant environment. Currently, the pick-up algorithm is tested in SITL and on the Solo UAV. Next stage is implementation and testing on the S1000 platform. The RBS needs to be upgraded so the arm mechanism is capable to lift and maneuver the MUG.

V. CONCLUSIONS

Combination of Unmanned Vehicles into systems-of-systems bring new opportunities to ocean exploration and research. In this paper we provided details of MUG deployment and recovery mechanism using a multirotor UAV. We provided details on MUG localization using computer vision and a custom marker. We used an alternative to a HSV filter-based approach for visual detection of "International Orange" objects on the surface of water. In field experiments we assessed a mechanical interface between MUG and UAV using EPM. We discussed RBS design where a robotic arm is used to store, manipulate MUGs, and attach them to the UAV.

REFERENCES

[1] E. Honoré-Livermore, R. Birkeland, and C. Haskins, "Addressing the sustainable development goals with a system-of-systems for monitoring arctic coastal regions," *INCOSE International Symposium*, vol. 30, no. 1, pp. 604–619, 2020. [Online]. Available: https://onlinelibrary.wiley.com/doi/abs/10.1002/j.2334-5837.2020.00743.x

[2] J. Pinto, M. Costa, K. Lima, P. Dias, J. Pereira, M. Ribeiro, R. Campos, Z. Mirmalek, R. Mendes, F. Castejón, J. Gilabert, M. P. Tomasino, C. Magalhães, J. da Silva, P. Relvas, T. Lukaczyk, K. Skarpnes, M. Ludvigsen, A. Chekalyuk, and K. Rajan, "To boldly dive where no one has gone before:experiments in coordinated robotic ocean exploration," 12 2020.

[3] J. Fortuna and T. A. Johansen, "A lightweight payload for hyperspectral remote sensing using small uavs," in *2018 9th Workshop on Hyperspectral Image and Signal Processing: Evolution in Remote Sensing (WHISPERS)*, 2018, pp. 1–5.

[4] C. Koparan, A. B. Koc, C. V. Privette, C. B. Sawyer, and J. L. Sharp, "Evaluation of a uav-assisted autonomous water sampling," *Water*, vol. 10, no. 5, 2018. [Online]. Available: https://www.mdpi.com/2073-4441/10/5/655

[5] A. Dallolio, B. Agdal, A. Zolich, J. A. Alfredsen, and T. A. Johansen, "Long-endurance green energy autonomous surface vehicle control architecture," in *OCEANS 2019 MTS/IEEE SEATTLE*, 2019, pp. 1–10.

[6] T. Howatt, J. Palter, R. Matthews, B. Deyoung, R. Bachmayer, and B. Claus, "Ekman and eddy exchange of freshwater and oxygen across the labrador shelf break," *Journal of Physical Oceanography*, vol. 48, 02 2018.

[7] A. Saad, A. Stahl, A. Våge, E. Davies, T. Nordam, N. Aberle, M. Ludvigsen, G. Johnsen, J. Sousa, and K. Rajan, "Advancing ocean observation with an ai-driven mobile robotic explorer," *Oceanography*, vol. 33, pp. 50–59, 09 2020.

[8] M. Ludvigsen, P. S. Dias, S. Ferreira, T. O. Fossum, V. Hovstein, T. A. Johansen, T. R. Krogstad, Ø. Midtgaard, J. S. P. Norgren, Ø. Sture, E. Vågsholm, and A. Zolich, "Autonomous network of heterogeneous vehicles for marine research and management," in *IEEE Oceans 2016 – Monterey, CA*, September 2016.

[9] E. I. Sarda and M. R. Dhanak, "A usv-based automated launch and recovery system for auvs," *IEEE Journal of Oceanic Engineering*, vol. 42, no. 1, pp. 37–55, 2017.

[10] O. M. Brokstad, R. Klæboe, E. Sollesnes, B. V gen, A. Carella, A. Alcocer, T. A. Johansen, and A. P. Zolich, "Towards the development of miniature underwater gliders with uav deployment/recovery capabilities," 2018.

[11] M. Elkolali, W. A. Splawski, A. Carella, and A. Alcocer, "Hydrodynamic parameter optimization for miniature underwater glider wings," in *Global Oceans 2020: Singapore – U.S. Gulf Coast*, 2020, pp. 1–8.

[12] J. Pinto, P. S. Dias, R. Martins, J. Fortuna, E. Marques, and J. Sousa, "The LSTS toolchain for networked vehicle systems," in *OCEANS - Bergen, 2013 MTS/IEEE*, June 2013, pp. 1–9.

[13] A. P. Antonio-Javier Gallego and P. Gil, "Automatic ship detection from optical aerial images with convolutional neural networks," *Remote Sensing*, vol. 10, no. 4, 2018.